Intraoperative Augmented Reality for Minimally Invasive Liver Interventions

Michael Scheuering[1], Andrea Schenk[2], Armin Schneider[3], Bernhard Preim[2], Günther Greiner[1]

[1]Computer Graphics Group, University of Erlangen-Nuremberg,
Am Weichselgarten 9, 91058 Erlangen, Germany
[2]MeVis - Center for Medical Diagnostic Systems and Visualization,
Universitaetsallee 29, 28359 Bremen, Germany
[3] Institute MITI, TU Munich, Trogerstrasse 26, 81675 Munich, Germany

ABSTRACT

Minimally invasive liver interventions demand a lot of experience due to the limited access to the field of operation. In particular, the correct placement of the trocar and the navigation within the patient's body are hampered. In this work, we present an intraoperative augmented reality system (IARS) that directly projects preoperatively planned information and structures extracted from CT data, onto the real laparoscopic video images. Our system consists of a preoperative planning tool for liver surgery and an intraoperative real time visualization component. The planning software takes into account the individual anatomy of the intrahepatic vessels and determines the vascular territories. Methods for fast segmentation of the liver parenchyma, of the intrahepatic vessels and of liver lesions are provided. In addition, very efficient algorithms for skeletonization and vascular analysis allowing the approximation of patient-individual liver vascular territories are included. The intraoperative visualization is based on a standard graphics adapter for hardware accelerated high performance direct volume rendering. The preoperative CT data is rigidly registered to the patient position by the use of fiducials that are attached to the patient's body, and anatomical landmarks in combination with an electro-magnetic navigation system. Our system was evaluated in vivo during a minimally invasive intervention simulation in a swine under anesthesia.

Keywords: Registration, image-guided surgery, direct volume rendering, hardware acceleration, computer assisted surgery

1. INTRODUCTION

The vascular anatomy, in particular the branching patterns of vasculature determines therapeutic decisions and the realization of therapy in the operating room. Therefore, vascular analysis based on volumetric datasets becomes more and more important.

Especially for oncologic resections in liver surgery, the spatial location of tumors and their relation to the main hepatic vessels and the parenchyma is essential. According to the complex anatomy of the liver, preoperative therapy planning and the intervention in the operation room demand a lot of practice to the surgeon. The introduction of a liver planning tool can assist the physician immensely, providing patient-individual analysis and visualization. Thus, it allows a 3D exploration of the patient's liver anatomy, tumor and vascular measurements. Additionally, the shape and the volume of vascular territories can be extracted, based on algorithms that take into account the intrahepatic vascular anatomy.

Although preoperative planning tools for liver surgery can assist the surgeon in an efficient way, a drawback is the lack of presence of planning data in the operation room during the intervention. Therefore, it is the surgeon's task to map the planning results on the intraoperative scene in mind. Especially in the context of minimally invasive procedures, this mapping becomes more complex, since the whole operation field can only be visualized

Further author information: (Send correspondence to M. Scheuering)
Phone: +49.9131.8529923
E-mail: scheuering@cs.fau.de
Web: http://www9.informatik.uni-erlangen.de/Persons/Scheuering

by means of a camera-monitor system. Additionally, the tissue of interest is only accessible via small surgical tools and depth information is completely lost.

A possible assistance for such intervention schemes is provided by *augmented reality systems* (ARS) that allow the projection of 3D information onto the real laparoscopic video streams, which can ease the navigation within the patient's body immensely. Additionally, the provision of preplanned 3D information into the surgeon's view allows to directly make use of the patient-individual liver analysis, which increases the available 3D information of a patient at intervention time.

In our work, we present such an ARS in terms of an image overlay system that directly projects patient-individual information, provided by HepaVision,[1] onto the real laparoscopic video images at real time frame rates. While the surgeon moves the laparoscopic camera, the virtual view including the preplanned 3D information, is adapted automatically.

This work is divided into the following sections. In Section 2 we give an overview of some previous work that is similar to our approach. In Section 3, an overview of our preoperative planning tool for liver analysis and its applied mechanisms and algorithms is presented. The rigid registration between the patient and the visualization system is explained in Section 4, whereas the necessary calibration steps such as lens distortion correction is presented in Section 5. Since the visualization of the presented 3D data has to be performed at real time frame rates, Section 6 introduces the techniques of our algorithms. Afterwards, some results are presented in Section 7. Finally, in Section 8 the work is concluded.

2. PREVIOUS WORK

Image overlay systems often have been used in different medical applications. The first important use was in neurosurgical interventions as proposed by Roberts *et al.*[2] Simple outlines or trajectories in one eyepiece have been overlaid, extracted from the original CT volume. Other systems use standard flat panel liquid crystal displays (LCD), whereas the visualization panel is tracked by an navigation system.[3] Alternatively, head-mounted displays (HMD) like the Varioscope System[4] are applied. For minimally invasive procedures, Fuchs *et al.*[5] developed an expensive 3D laparoscope, consisting of a projector for structured light for depth calculation of the inner organs. The augmentation of the surgeon's view is realized by the use of a tracked HMD. A complete visualization platform for image overlay has been proposed by Shahidi *et al.*,[6] including intraoperative navigation of the surgical tools and OpenGL-based visualization for the image overlays, which is similar to our system. All presented systems apply a rigid body registration in order to match the patient and the visualization system.

There are also systems for non-linear registration between the liver and the preoperative CT in order to assist open liver surgery.[7] Here, the registration is performed by the introduction of Doppler ultrasound and electro-magnetic navigation.

Although all mentioned techniques provide the possibility for image overlay or augmentation, there is a lack of systems for minimally invasive liver interventions that merge the power of intraoperative augmented reality and special purpose preoperative planning results.

3. PREOPERATIVE PLANNING

For therapies in liver tumor treatment, preoperative planning requires detailed knowledge about the patient's anatomy. The spatial relations between pathological and vital structures are essential for estimating the risks of minimally invasive and surgical treatment. For conventional surgery, a resection proposal has to fully enclose the tumors to be removed, whereas main branches of the vascular systems must be preserved. This guarantees that the remaining functional part of the liver is sufficient for the patient's survival. If a surgical resection proves impossible as a result of either a tumors location or the patient's constitution, the destruction of a tumor by minimally invasive interventions or thermal ablations, such as laser-induced thermotherapy (LITT) or radio-frequency ablation (RF), often is a viable alternative. However, profound planning is even more important for minimally invasive therapies than in conventional surgery. On one hand, vascular territories have to be respected as well, while on the other hand, there is a lack of visual control of the ongoing therapy due to limitations of intraoperative imaging. Moreover, minimally invasive strategies require planning of the instruments' trajectories to ensure that major vascular branches are not violated.

The preoperative planning in this project is based on contrast enhanced CT data and consists of several segmentation and image analysis steps:

- Segmentation of the liver
- Segmentation of liver tumors
- Segmentation of hepatic vessels
- Structural analysis of hepatic artery, portal vein and hepatic veins
- Calculation of vascular territories and risk analysis

These steps are all part of the software assistant HepaVision and described in detail in the following subsections.

3.1. Liver Segmentation

The liver is neighbored to other anatomical structures with similar density values (heart, stomach). This causes problems for fully-automatic segmentation approaches and is the reason why in most hospitals the liver boundaries are manually defined by contour tracing. As a compromise between unsuccessfull automatic and time-consuming manual segmentation, we perform the definition of liver contours with a modified live-wire method, a semi-automatic edge-oriented algorithm.[8,9] With live-wire the user starts with selecting a first contour point and moves a pointing device (for example a mouse) to roughly sketch the object's contour. The algorithm relies on a cost-function to calculate an optimal path between the start point and the current position of the pointing device in real-time. The cost-function is a weighted sum considering the magnitude of the gradient, the direction of the gradient and the laplacian zero-crossing. With this approach, a few user-defined contour points lead to a piece-wise optimal user-steered segmentation.

The initial approach has been carefully refined in order to enhance 3D segmentation. For this purpose, we combined live-wire with shape-based interpolation[10] between interactively segmented contours and subsequent optimization. This new approach computes the majority of the contours automatically and therefore reduces the interaction effort.[8,11] Interactive modification of the interpolated contours, however, is still possible. With this approach the user can steer the segmentation process and generate precise results in acceptable time.

3.2. Tumor Segmentation

The segmentation of a liver tumor from CT data requires different tools depending on the type of the lesion. Therefore, more than one tool is offered for this image processing step. While the segmentation of metastasis can be performed in most cases with a simple region-growing or a watershed algorithm, the extraction of hepatocellular carcinoma is more elaborate. For example, after chemoembolisation with Mitomycin and Lipiodol these lesions appear in the data as inhomgenious, hyperdense regions. Here, a modified algorithm based on Fuzzy-Connectedness[12,13] showed promising results. In cases where the automatic or semi-automatic approaches fails, a live-wire or manual delineation tool can be used. For larger lesions, the interpolation method described in the last subsection is applied. The segmentation of tumors at the boundary of the liver is simplified by restricting it to the liver mask, allowing the user to draw the outer contours very roughly.

3.3. Vascular Segmentation

The segmentation of the intrahepatic vessels is a prerequisite for a subsequent geometrical and structural analysis. In a preprocessing step, filter functions for noise reduction (Gaussian, median filter) and for background compensation (Laplace-like filters) are applied to the CT-data.[14] As a result, intrahepatic vessels can be identified and delineated by use of a threshold-based region-growing method. Usually, region-growing segmentation must be repeated with modified thresholds until an appropriate result is found. To accelerate this procedure, we refined it to suggest a threshold automatically.[14] The new algorithm works as follows.

Initially, a seed voxel is selected interactively in the portal vein at the liver hilum. Starting with this seed voxel, the region-based segmentation algorithm iteratively accumulates the 26 adjacent voxels with an intensity

equal to or greater than the intensity θ_{beg} of the seed voxel and keeps them in a list $L(\theta_{beg})$. Using $L(\theta_{beg})$ as new seed voxels, all adjacent voxels with intensities greater or equal $\theta_{beg} - 1$ are collected in a list $L(\theta_{beg} - 1)$. The threshold is further decreased until a given threshold θ_{end} is reached which creates only voxels $L(\theta_{end})$ outside the vascular systems. The automatic threshold selection is based on the observation that the number of voxels $N(\theta)$ is approximately linear decreasing for $\theta = \theta_{opt} \ldots \theta_{beg}$. At θ_{opt} the slope changes considerably because many voxels belonging to the liver tissue are collected for thresholds below θ_{opt}. A suggestion for θ_{opt} can thus be found by calculating an optimal fit of two straight lines for $N(\theta)$. If the suggested threshold is not satisfying it may be adjusted interactively. New segmentation results are displayed immediately using the voxel lists already created.

3.4. Vascular Analysis

The segmentation result is a set of voxels representing the intrahepatic vascular systems. For surgery planning, a further analysis of these voxels is required. This includes geometric measurements of the branches (radius, length), the identification of individual vascular systems and the identification of the ramification pattern (e.g. to determine the main portal subtrees supplying the liver segments).

Depending on the scanning protocol, usually two or more different vascular systems of the liver are enhanced with contrast agent during the scan. Often the portal vein and hepatic veins are affected. Therefore, the scan yields high-intensity voxels for both vascular systems. Due to the limited spatial resolution of the scanned volume data, voxels of different vascular systems are often adjacent to each other such that they are segmented as one object when in reality there is only proximity between the two. We analyze and separate such "forests" of connected vascular systems automatically using graph theoretical methods. In a first step, the voxel-based shape representation of the vessels is transformed into an abstract graph representation, utilizing "skeletonization".[15] The skeleton representation enables a much easier access to the geometry of the branches and to structural information (ramifications).

The separation of vascular systems is based on the model assumption that the cross section of a vascular tree becomes smaller towards the periphery. If two adjacent branches of the vascular tree have strongly different diameters and the branch with larger distance to the tree has the larger diameter then we have a candidate for the separation of the vascular tree. If the automatic vessel separation does not succeed completely, interaction facilities can be used to manually set the root of a vascular system or to identify touching points. The graph representation of the vessels is also the basis for user interactions such as defining the hierarchical structure of trees, subtrees and paths. Furthermore it allows to measure the radius, length or volume of branches.The main branches of the portal vein were identified automatically by determining the 8 most voluminous subtrees, which are assumed to supply the various vascular territories roughly corresponding to Couinaud[16] liver segments.

3.5. Vascular Territories and Risk Analysis

For liver surgery, the knowledge of the shape and volume of the patient's vascular territories is essential to estimate the risk of different resection strategies. Due to the limited spatial resolution only the major branches of the portal vein can be extracted. Referring to the liver, the problem can be described as follows: Assume that L is the set of all voxels in the medical volume data representing the liver. Furthermore, let $B \subset L$ denote the set of voxels belonging to the extracted portal venous tree. B is the union of the main branches or subtrees $B_i \subset B$, $i = 1, ..., n$, which supply the portal venous territories. To determine the vascular territories, we have to find a function which assigns to each liver voxel $\in L$ a territory with number i, provided it is supplied by the branch B_i.

The definition of a realistic function must reflect the probability, that the sprouts of the various incomplete subtrees B_i reach and supply a certain liver voxel. Measures for this 'reachability' can be expressed by a metric. A voxel then is assigned to that branch B_i, which has the shortest distance with respect to a suitable metric. The choice of a metric is difficult since the blood supply is realized by complex branching structures, whose formation process is not fully understood. After carefully evaluating two different metrics[17] we chose the Euclidean distance metric. With respect to the number of voxels assigned correctly, similar results were achieved with both metrics. The Euclidean distance, however, is better suited for the requirements of the clinical routine since it is computationally fast.

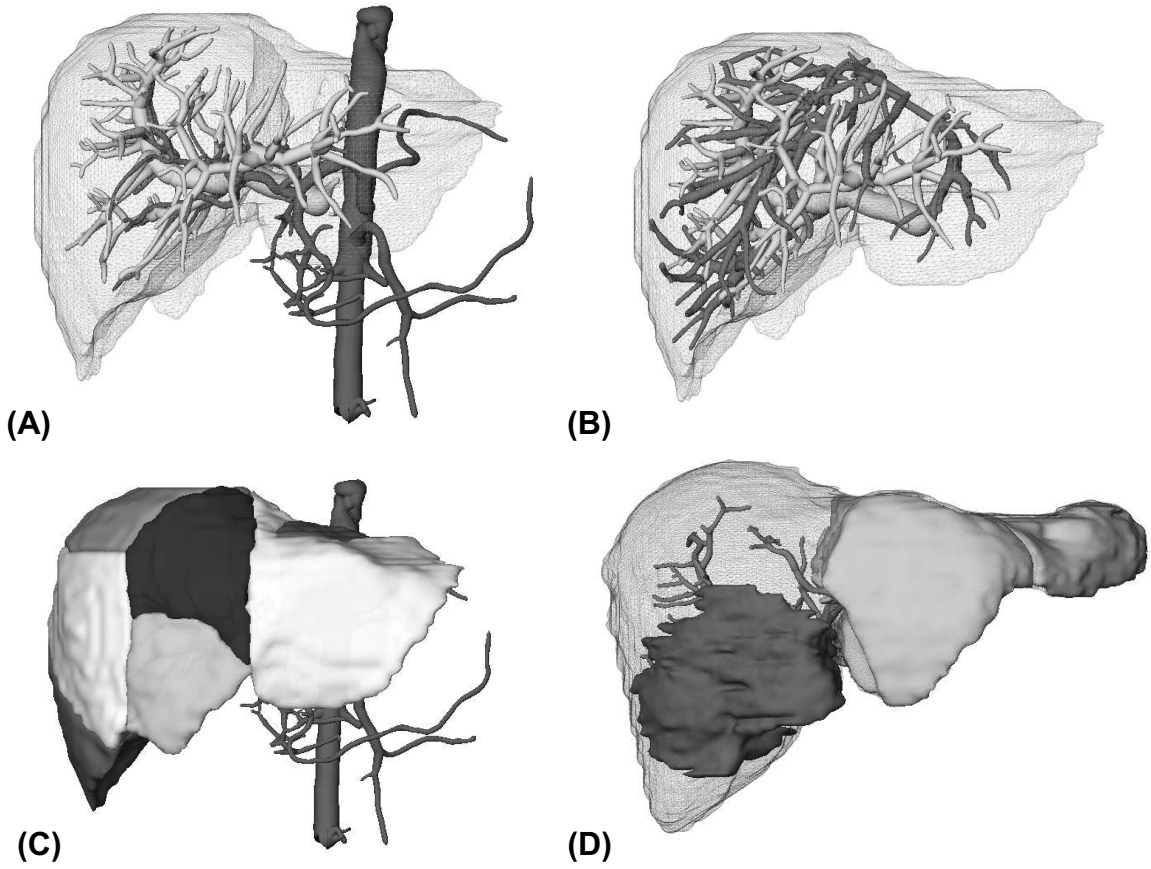

Figure 1. Example images of HepaVision: (A) presents the portal vein and the hepatic artery of a patient's liver. (B) visualizes the portal vein and hepatic veins. (C) shows the vascular territories. (D) presents the portal vein, a large tumor (dark) and the segments being not at risk by insufficient blood supply caused by the planned tumor resection. The dataset (A)-(C) have been provided by the Lahey Clinic Boston and (D) by the Technical University of Munich, Radiology.

In patients with liver tumors a risk analysis is performed. Risk analysis includes the identification of vessels within a safety margin around a tumor and the depending vessels in the periphery. Subsequently, the territory which is supplied by all involved vessels is calculated. This area is highlighted in the visualization and its volume (as absolute value and as percentage of the total liver volume is shown). The quantification and visualization of the parenchyma at risk is a valuable support for the surgical decision about resectability. This procedure is described in detail in.[18]

3.6. Implementation

All necessary image processing steps are performed with ILAB4, a R&D platform for image processing and visualization developed at MeVis. With ILAB4, modules, each representing an image processing task, are combined graphically to create specialized networks that perform a well defined task. By means of a scripting language a graphical user interface (GUI) can easily be composed. The user interface contains only a subset of the control elements available in the underlying image processing modules. These control elements are carefully chosen to reflect the most frequently needed parameters. Thus, the complexity of the underlying image processing networks are hidden from the user. Also, the user is guided through all necessary processing steps by the GUI.

All segmentation results are managed by HepaVision. For this purpose, a data structure has been developed which uses the syntax of the wide-spread XML-format (Extended Markup Language). By choosing XML it is possible to import the results of the planning process into other tools. In each processing step the GUI consists

of two large displays for image data and one region where the control elements are provided. The display regions may be used to display 2D slice data as well a 3D visualization with the usual facilities to control (zoom and rotate) the virtual camera. It is possible to superimpose the segmentation results to the original slice data.

3.7. Clinical Evaluation

In addition to the anatomical validation, our methods have been evaluated in the clinical environment for more than 220 cases until now (at Medical School Hannover, at University Hospital Essen, at the Institute MITI in Munich and others). The system is also used for living donor liver transplantations in the Lahey Clinic Boston and the Kyoto University Hospital.

For the planning of liver resections in patients with liver tumors, the liver, tumors, arteries, portal vein and hepatic veins were extracted from CT-data and visualized in 3D with our software assistant HepaVision. It has been shown that these visualizations allow a suitable interactive planning of liver resections and improve the preparation especially of complex liver resections.[19] Surgeons at Medical School Hannover regularly use the 3D reconstruction and volumetric analysis for the preoperative planning of living donor liver transplantations.[20,21] The vascular anatomy is crucial in the evaluation of potential donors.

For the acceptance in a clinical setting, the time required to carry out the image analysis is important. Using the feedback provided by the clinical partners, HepaVision has been improved significantly over the last four years and migrated from Silicon Graphics Hardware to Windows-based PCs. In this process, the graphical user interface, the facilities to generate visualizations and animation sequences have been enhanced. With the current version, preoperative planning takes an experienced user an hour on average for oncologic cases and 45 minutes for planning of LRLT where tumor segmentation and risk analysis are not relevant. Some results are presented in Figure 1.

4. REGISTRATION

In order to register the patient to the visualization system for generation of the video overlays, which will be described in Section 6, we use plastic fiducial markers that are attached to the patient's body and anatomical landmarks. Since the fiducials have to be identified both on the patient's surface and within the CT volume, we use an electro-magnetic navigation system (Ascension^{TM} miniBird 800, 6 degrees of freedom, with a $8mm \times 8mm \times 18mm$ sensor), but optical tracking (NDI^{TM} Polaris) would also be possible. For realization in the operation room, the sensor of the navigation system is fixed to the laparoscopic camera for image guidance such that a sterile plastic wrapping of the camera during the intervention is possible.

For registration purposes N pairs of points $(p^i_{patient}, p^i_{CT}), i = 1...N$ are collected. Then a rigid body registration by the use of the Singular Value Decomposition[22] (SVD) is applied.

5. CALIBRATION

Modern video-based endoscopes or laparoscopes offer physicians a field of view that is wide angled which is imperative for minimally invasive interventions. Unfortunately, this causes heavy lens distortion effects, mostly of radial and tangential type. In order to guarantee correct video overlays, one has to calculate a projective 3D/2D mapping that maps 3D object points $\mathbf{p}^W_{3D}$, defined in world coordinates, to 2D image points $\mathbf{p}^I_{2D}$, which are defined in the image plane of the camera (notation in homogenous coordinates):

$$\mathbf{p}^I_{2D} = \mathbf{P}^{\in \mathcal{R}^{3\times 4}} \cdot \mathbf{T}^{\in \mathcal{R}^{4\times 4}} \cdot \mathbf{p}^W_{3D} \tag{1}$$

This requires the determination of a projective matrix $\mathbf{P}^{\in \mathcal{R}^{3\times 4}}$, whose elements can be determined by standard camera calibration routines.[23] Object rotation and translation is considered by matrix $\mathbf{T}^{\in \mathcal{R}^{4\times 4}}$. In order to apply OpenGL 3D renderings in an efficient way, lens distortion correction has to be considered. Therefore, we implemented a fast hardware accelerated correction method, which divides a video image into $N \times M$ patches. By means of 2D texture mapping, each texture coordinate $\mathbf{t}^i$ is assigned a vertex coordinate $\mathbf{v}^i$ (Figure 2):

$$\mathbf{t}^i = (x, y)^T = F((x', y')^T) = F(\mathbf{v}^i) \tag{2}$$

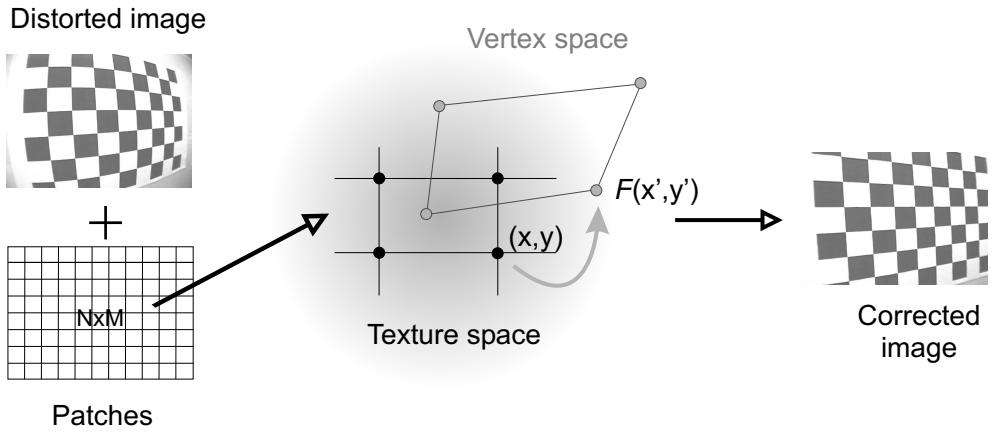

Figure 2. Lens distortion correction by the use of OpenGL hardware acceleration and 2D texture mapping.

The polynomial function F is determined by camera calibration.[23] For $N = M = 32$ patches we achieved high image quality at real time frame rates. Finally, the tip transformation of the tracker's sensor to the optical center of the camera is calculated by a hand-eye calibration procedure.[24]

6. VISUALIZATION

There is a variety of different visualization approaches for scalar volumes in many different applications. Since we want to present 3D volumes, extracted from our preoperative planning tool, in a semitransparent manner in order to enhance depth information, we only apply *direct volume rendering* methods that immediately display the voxel data. Although approaches like standard software *raycasting*[25] provide powerful visualization nowadays, hardware accelerated texture-based techniques based on new graphics adapters have been successfully developed for medical visualization.[26–29]

2D texture-based approaches allow direct volume rendering in terms of object-aligned slices. By changing the viewing direction of more than 90 degrees, a new stack of slices has to be applied, blended in back-to-front order and bilinear interpolation within the slices. The main drawback of such methods is the lack of spatial interpolation. The standard in texture-based approaches in terms of image quality has been provided by Cabral *et al.*[26] utilizing 3D textures and viewport-aligned slices, blended in back-to-front order. Hereby, trilinear interpolation in hardware is responsible for filling in the slicing polygons. On changing the camera view, the polygons have to be recalculated.

By the introduction of *multi-texturing* and a *programmable multi-stage rasterization* hardware, 2D multi-textures are superior to 3D textures in terms of frame performance.[30] Multi-texturing which is defined in recent standard API releases like *DirectX* or *OpenGL*, provide the capability to assign one polygon to several textures within the rendering-pipeline (Figure 3 (A)). In our approach, the resulting attributes of a single fragment (pixel values of geometric primitives) such as color or opacity are determined, using programmable arithmetic operations during rasterization. These operation schemes, such as the *Register Combiners* from NVIDIA^{TM} GeForce cards or the *Fragment Shaders* from ATI^{TM} Radeon allow to completely bypass the standard texturing unit. In combination with multi-textures, trilinear interpolation can be efficiently calculated in hardware (Figure 3 (B)). If S_i and S_{i+1} are two volume slices then the intermediate slice $S_{i+\alpha}$ can be calculated by

$$S_{i+\alpha} = (1 - \alpha) \cdot S_i + \alpha \cdot S_{i+1}. \tag{3}$$

Additionally, programmable multi-stage rasterization allows to introduce for example the *Phong* local illumination model or non-polygonal isosurfaces at high frame rates.[28,29] Thus, this approach is the visualization system of choice, since high image quality for tumors and vessels at interactive frame performance is requested for image overlay. Additionally, stereo rendering is also applicable in conjunction with standard shutter glasses.

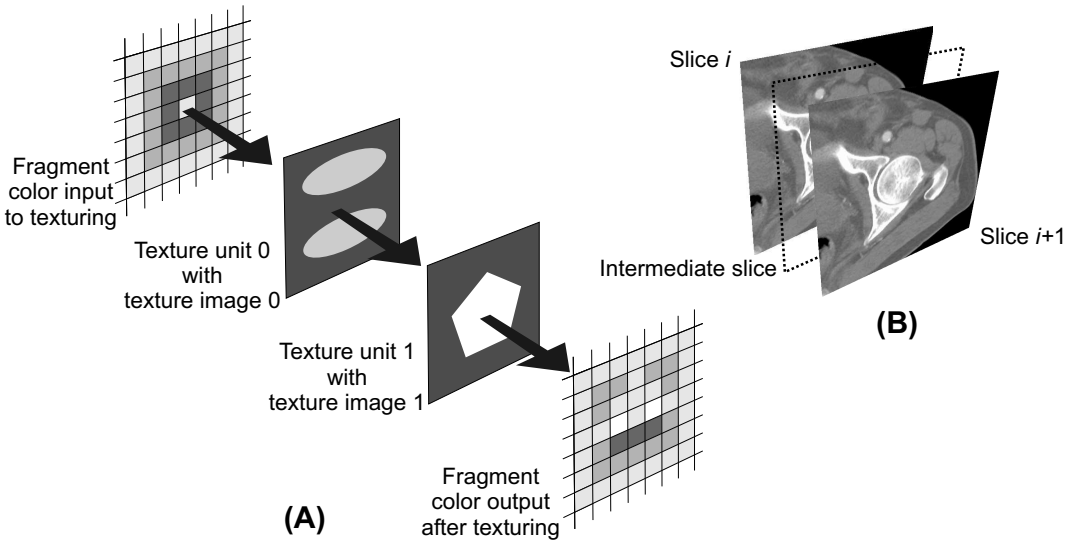

Figure 3. Interpolation of an intermediate volume slice by multi-texturing techniques: A) shows the process of multi-texturing by assigning one polygon several textures, B) intermediate slice interpolation in hardware.

7. RESULTS

Our system was evaluated in vivo during a simulated minimally invasive intervention in a swine. The medical work flow was similar to a liver intervention, which is one possibility to get advantage from the ARS. In our case, a routine abdominal CT of the swine was acquired using contrast agent for enhancement of the vessels. The following preoperative analysis and planning was accomplished within less than one hour, using the techniques presented in Section 3. The resulting anatomical information (liver, portal venous and hepatic venous trees, vascular territories) was used for insertion of the Veress needle in order to generate the pneumoperitoneum (Figure 4 (A)(B)(C)), for trocar placement, and for intraoperative navigation during intervention (Figure 4 (D)). The applied data volume was of dimension $512 \times 512 \times 90$ with 3mm slice thickness at 25 fps (3D video overlay by the use of the multi-texture-based direct volume rendering (Section 6) and lens distortion correction (Section 5)). For rigid registration purposes (Section 4) only four fiducial landmarks are necessary in order to achieve 5mm of overlay accuracy. Since the system has been evaluated in a swine in vivo, the planning procedure, especially the vascular segmentation and analysis was hampered by breathing artifacts during the CT scan. Nevertheless, in real therapy work flows, this does not provide a problematic circumstance.

8. CONCLUSION

Using our high performance volume rendering system based on general purpose hardware, we are capable of augmenting the surgeons laparoscopic view at real time frame rates. In combination with the preoperative liver planning tool, which performs a dedicated liver vascular analysis, an intraoperative fusion of preplanned information and real laparoscopic images is possible. Additionally, for visualization, all combinations of anatomical structures or intervention plans are feasible, depending on the surgeons requests. Moreover, the system is also applicable for many other intervention schemes such as radiofrequency (RF) ablation, percutaneous ethanol injection therapy (PEIT) and hepatic or pancreatic resections. According to the registration error, arising from the soft tissue movement of the liver, one can introduce a method for non-linear registration.[7, 31]

ACKNOWLEDGMENTS

We would like to thank H. Barfuss, C. Rezk-Salama and H. Feussner for fruitful scientific discussions.

REFERENCES

1. H. Bourquain, A. Schenk, F. Link, B. Preim, G. Prause, and H.-O. Peitgen, "Hepavision2: A software assistant for preoperative planning in living-related liver transplantation and oncologic liver surgery," in *Computer Assisted Radiology and Surgery, Proc. CARS*, pp. 341–346, 2002.
2. D. W. Roberts, J. W. Strohbehn, J. F. Hatch, W. Murray, and H. Kettenberger, "A frameless stereotaxic integration of computerized tomographic imaging in the operating microscope," *Journal of Neurosurgery* **65**, pp. 545–549, 1986.
3. M. Blackwell, C. Nikou, A. M. DiGioia, and T. Kanade, "An image overlay system for medical data visualization," in *Proc. Medical Image Analysis (SPIE)*, pp. 67–72, 2000.
4. W. Birkfellner, M. Figl, K. Huber, F. Watzinger, F. Wanschitz, R. Hanel, A. Wagner, D. Rafolt, R. Ewers, and H. Bergmann, "The varioscope ar - a head-mounted operating microscope for augmented reality," in *MICCAI*, pp. 869–877, 2000.
5. H. Fuchs, M. A. Livingston, R. Raskar, D. Colucci, K. Keller, A. State, J. R. Crawford, P. Rademacher, S. H. Drake, and A. A. Meyer, "Augmented reality visualization for laparoscopic surgery," in *MICCAI*, pp. 934–943, 1998.
6. R. Shahidi, B. Wang, M. Epitaux, J. Adler, and G. Steinberg, "Intraoperative video and volumetric image fusion," in *CARS*, 1999.
7. M. Vetter, P. Hassenpflug, I. Wolf, M. Thorn, C. Cárdenas, L. Grenacher, G. M. Richter, W. Lamadé, M. W. Büchler, and H.-P. Meinzer, "Intraoperative Navigation in der Leberchirurgie mittels Navigationshilfen und Verformungsmodellierung," in *Bildverarbeitung für die Medizin 2002*, pp. 73–76, 2002.
8. A. Schenk, G. Prause, and H.-O. Peitgen, "Efficient semiautomatic segmentation of 3d objects in medical images," in *Medical Image Computing and Computer-Assisted Intervention – MICCAI 2000*, **1935**, pp. 186–195, 2000.
9. A. X. Falcao, K. Jayaram, J. K. Udupa, and F. K. Miyazawa, "An ultra-fast user-steered image segmentation paradigm: Live-wire-on-the-fly," in *Medical Imaging: Image Processing, Proc. SPIE* **3661**, pp. 184–191, 1999.
10. S. P. Raya and J. K. Udupa, "Shape-based interpolation of multidimensional objects," *IEEE Transactions on Medical Imaging* **9**(1), pp. 32–42, 1990.
11. A. Schenk, G. Prause, and H.-O. Peitgen, "Local cost computation for efficient segmentation of 3d objects with live wire," in *Medical Imaging: Image Processing, Proc. SPIE* **4322**, pp. 1357–1364, 2001.
12. J. K. Udupa, S. Samarasekera, and W. A. Barrett, "Boundary detection via dynamic programming," in *Visualization in Biomedical Computing '92*, pp. 1087–1091, 1992.
13. A. Schenk, S. Behrens, S. A. Meier, P. Mildenberger, and H.-O. Peitgen, "Segmentierung von Hepatozellulaeren Karzinomen mit Fuzzy-Connectedness," in *Bildverarbeitung für die Medizin*, 2003. to appear.
14. D. Selle, B. Preim, A. Schenk, and H.-O. Peitgen, "Analysis of vasculature for liver surgery planning," *IEEE Transactions on Medical Imaging* **21**(11), 2002. to appear.
15. D. Selle and H.-O. Peitgen, "Analysis of the morphology and structure of vessel systems using skeletonization," in *Medical Imaging: Physiology and Function from Multidimensional Images, Proc. SPIE* **4321**, pp. 271–281, 2001.
16. C. Couinaud, "Le foie. etudes anatomiques et chirurgicales," 1957.
17. J. H. D. Fasel, D. Selle, C. J. G. Evertsz, F. Terrier, and H.-O. Peitgen, "Segmental anatomy of the liver: Poor correlation with CT," *Radiology* **206**, pp. 151–156, 1998.
18. B. Preim, H. Bourquain, K. J. O. D. Selle, and H.-O. Peitgen, "Resection proposals for oncologic liver surgery based on vascular territories," in *Computer Assisted Radiology and Surgery, Proc. CARS*, pp. 353–358, 2002.
19. D. Hoegemann, G. Stamm, H. Shin, K. J. Oldhafer, H. J. Schlitt, D. Selle, and H.-O. Peitgen, "Individuelle Planung leberchirurgischer Eingriffe an einem virtuellen Modell der Leber und ihrer Leitstrukturen," *Radiologe* **40**, pp. 267–273, 1999.
20. D. Hoegemann, G. Stamm, K. J. Oldhafer, D. Selle, T. Schindewolf, and M. Galanski, "Volumetric evaluation and 3d-visualization of the liver before living-related donation," in *Computer Assisted Radiology and Surgery, Proc. CARS*, pp. 249–252, 1999.

21. B. B. J. Frericks, F. C. Caldarone, A. Schenk, D. Selle, B. Preim, H.-O. Peitgen, M. Galanski, B. Nashan, and J. Klempnauer, "New computational methods for the evaluation of living related liver donation," in *American Journal of Transplantation*, **1**, p. 209, 2001.
22. W. H. Press, S. A. Teukolsky, W. T. Vetterling, and B. P. Flannery, *Numerical Recipes in C*, Cambridge University Press, 2nd ed., 1992.
23. R. Tsai, "A versatile camera calibration technique for high-accuracy 3D machine vision metrology using off-the-shelf TV cameras and lenses," *IEEE Journal of Robotics and Automation* **3**, pp. 323–344, 1987.
24. R. Y. Tsai and R. K. Lenz, "A new technique for fully autonomous and efficient 3D robotics hand/eye calibration," *IEE Transactions on Robotics and Automation* **5**(3), pp. 345–358, 1989.
25. P. Lacroute and M. Levoy, "Fast volume rendering using a shear-warp factorization of the viewing transformation," in *Proc. of SIGGRAPH '94*, pp. 451–458, 1994.
26. B. Cabral, N. Cam, and J. Foran, "Accelerated volume rendering and tomographic reconstruction using texture mapping hardware," in *Proc. of 1994 Symposium on Volume Visualization*, pp. 91–98, 1994.
27. R. Westermann and T. Ertl, "Efficiently using graphics hardware in volume rendering applications," in *Proc. of SIGGRAPH, Comp. Graph. Conf. Series*, pp. 169–177, 1998.
28. C. Rezk-Salama, K. Engel, M. Bauer, G. Greiner, and T. Ertl, "Interactive volume rendering on standard PC graphics hardware using multi-textures and multi-stage rasterization," in *Proc. SIGGRAPH/Eurographics Workshop on Graphics Hardware*, pp. 109–118, 2000.
29. C. Rezk-Salama and M. Scheuering, "Multitexturbasierte Visualisierung in der Medizin," in *Bildverarbeitung für die Medizin 2001: Algorithmen, Systeme, Anwendungen*, pp. 137–141, Springer, 2001.
30. C. Rezk-Salama, *Volume rendering techniques for general purpose graphics hardware*. PhD thesis, University of Erlangen-Nuremberg, Computer Graphics Group, 2002.
31. M. Scheuering, C. Rezk-Salama, H. Barfuss, A. Schneider, and G. Greiner, "Augmented reality based on fast deformable 2D-3D registration for image-guided surgery," in *SPIE Medical Imaging*, pp. 436–445, 2002.

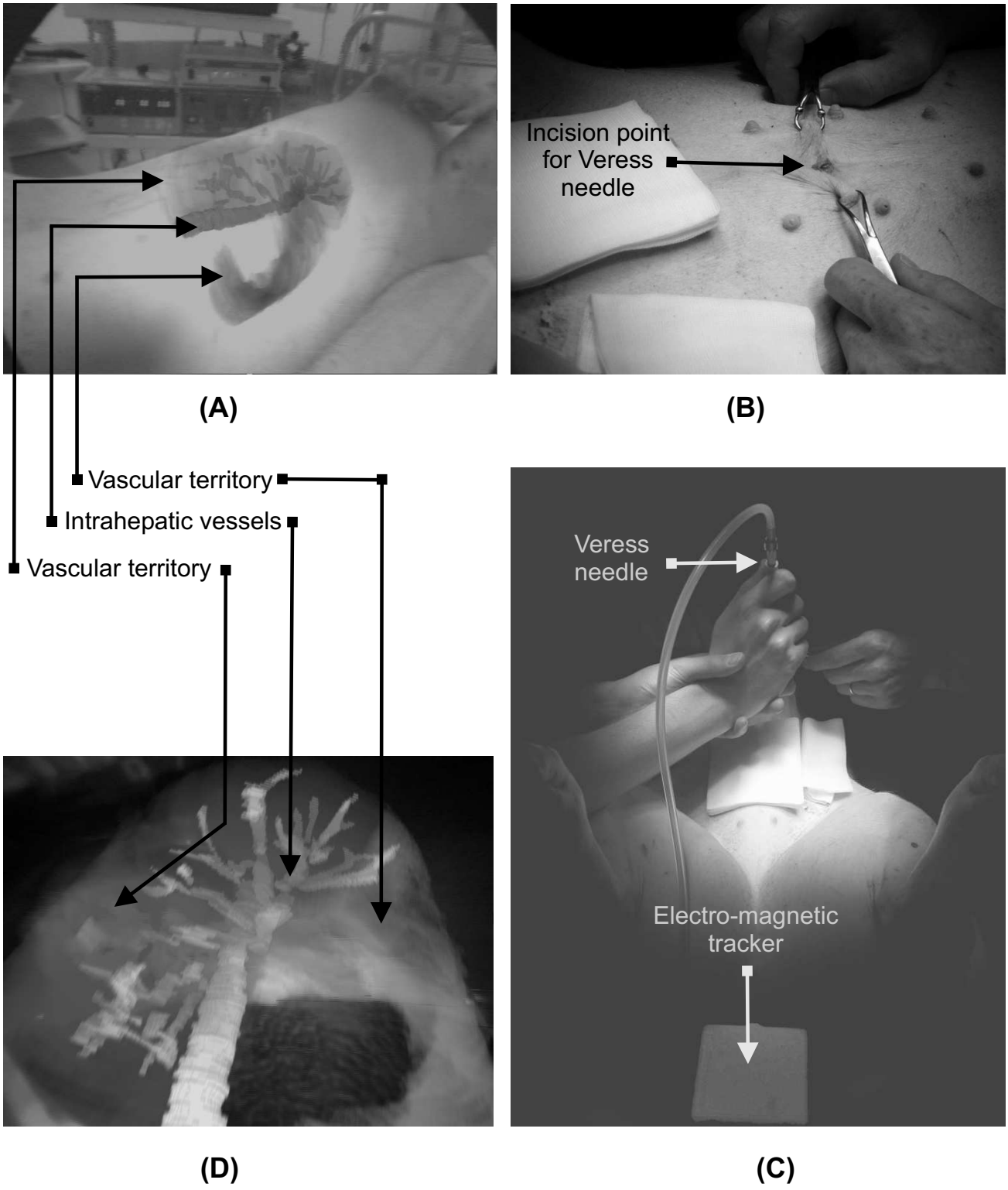

Figure 4. Results of a minimally invasive intervention simulation in a swine: (A) Shows intrahepatic vessels and liver segment overlay for Veress needle insertion. (B) Incision point of the Veress needle according to video overlays. (C) Insertion of the Veress needle for generation of the pneumoperitoneum. (D) Video overlay of a laparoscopic liver image with 3D renderings from our preplanning tool.